Available online at www.sciencedirect.com

SciVerse ScienceDirect

Ceramics International 39 (2013) 3017–3025

CERAMICS INTERNATIONAL

www.elsevier.com/locate/ceramint

Microstructure and mechanical properties of MgO–C refractories containing graphite oxide nanosheets (GONs)

Tianbin Zhu, Yawei Li*, Ming Luo, Shaobai Sang, Qinghu Wang, Lei Zhao, Yuanbing Li, Shujing Li

The Key State Laboratory Breeding Base of Refractories and Ceramics, Wuhan University of Science and Technology, Wuhan 430081, PR China

Received 20 August 2012; received in revised form 21 September 2012; accepted 21 September 2012
Available online 3 October 2012

Abstract

MgO–C refractories containing graphite oxide nanosheets (GONs) and Al, Si additives were prepared in this work. Firstly the MgO–GONs composite powders were fabricated by common ball milling of expanded graphite and magnesia powders, and then incorporated into MgO–C refractories. The phase composition, microstructure, mechanical and thermo-mechanical properties of MgO–C refractories treated at the different temperatures were investigated by means of X-ray diffraction (XRD), scanning electron microscopy (SEM) coupled with energy dispersive X-ray spectroscopy (EDS), three-point bending method and thermal shock test. The results showed that the GONs of different sizes and thicknesses were well distributed in magnesia powders. Addition of GONs had a positive influence on the mechanical properties of MgO–C refractories. After firing at 1400 °C, much higher cold modulus of rupture (CMOR) and increased displacement were achieved for MgO–C specimens with GONs added compared to that of the specimen contained only flaky graphite. Moreover, the thermal shock resistance of all the specimens containing GONs was better than that for the specimen containing no GONs. It was suggested that GONs and in-situ formed ceramic phases in the matrix strengthened and toughened MgO–C refractories.

Keywords: C. Mechanical properties; C. Thermal shock resistance; GONs; MgO–C refractories

1. Introduction

MgO–C refractories have been extensively used as the lining of basic oxygen furnaces (BOF), electric arc furnaces (EAF), ladles and RH vessels in steel-making process because of their excellent thermal, mechanical and chemical properties [1–3]. With the progress in clean steel technology and requirements of low carbon society, the conventional high carbon refractories (12–18 wt% C) need to be replaced by low carbon refractories. However, mechanical properties of the refractories will be adversely affected by the decrease in carbon content in the matrix, especially with respect to their thermal shock resistance. So, addition of nano-sized carbon and optimization of the microstructure have been considered in an attempt to enhance the performance of the low carbon refractories. Tamura et al. proposed the concept of nano-structured matrix for low carbon MgO–C refractories based on carbon black [4–6]. For instance, MgO-rimmed MgO–C refractories with nano-structured matrix containing hybrid graphitic black with B_4C were developed and showed both excellent thermal shock resistance and oxidation resistance [7]. Also, Nano-tech MgO–C bricks containing 4 wt% or 6 wt% flaky graphite had been developed with better corrosion resistance and thermo-mechanical properties compared to the conventional high carbon refractories (18 wt% C) [8]. Bag et al. reported that MgO–C containing 3 wt% flaky graphite and 0.9 wt% nano-sized carbon had the best combination of properties [9]. In addition, an approach of addition of micro-/nano-powders and formation of in-situ composites was adopted to improve the performance of MgO–C refractories [10–15]. Aneziris et al. [10] studied MgO–C compositions with TiO_2 or TiO_2/Al added, and discovered that their additions led to the formation of TiCN and TiC, respectively, which improved the oxidation resistance, mechanical strength

*Corresponding author. Tel.: +86 27 68862188; fax: +86 27 68862018.
E-mail addresses: liyawei@wust.edu.cn, liyaweiwust@hotmail.com (Y. Li).

0272-8842/$ - see front matter © 2012 Elsevier Ltd and Techna Group S.r.l. All rights reserved.
http://dx.doi.org/10.1016/j.ceramint.2012.09.080

as well as abrasion resistance of the bonding matrix. Ma et al. [14] also found that the slag penetration and corrosion resistance of the low-carbon MgO–C refractories can be remarkably improved by adding the synthesized Al_2O_3–SiC composite due to the increase of slag viscosity and the formation of $MgAl_2O_4$.

More recently, as new forms of nano-sized carbon, graphene or graphite oxide nanosheets (GONs) have been used to improve the performance of the polymer composites as well as ceramic matrix composites due to their unique mechanical, thermal and electrochemical properties [16–21]. For instance, a fracture toughness of 5.21 MPa $m^{1/2}$ has been obtained for the graphene nanosheets/alumina composites, representing an increase of 53% over that for the pure alumina material (3.40 MPa $m^{1/2}$) [19]. Furthermore, the multilayer graphene platelets/Si_3N_4 composites have been processed with increased bending strength and elastic modulus [21]. So, in the present work, an attempt was made to add GONs into MgO–C refractories and to investigate its effects on microstructure, mechanical and thermo-mechanical properties with an aim to explore the feasibility of using the GONs to enhance the performance of low carbon MgO–C refractories.

2. Experimental

2.1. Preparation of MgO–GONs composite powders

The expanded graphite (EG) was prepared by microwave irradiation in short time (20 s) using as-received expandable graphite (50 mesh, 96 wt% fixed carbon, Qingdao, China). The different amounts of as-prepared EG and MgO powders (~45 μm, 98 wt%, Dashiqiao, China) were mixed and wet-milled at a rotating speed of 400 r/m in a planetary ball mill using N-methyl pyrrole (NMP) as disperse media for 7 h (corundum balls as the abrasive media). The mass ratio of corundum balls to the powder mixtures was 1:1. After ball milling, the composite powder was dried at 60 °C for 120 h and then ground into fine powders. The mixing ratios of magnesia powders to EG were 100:0, 100:2, 100:5, 100:8, and 100:10, which were designated as GON0, GON2, GON5, GON8 and GON10, respectively.

2.2. Preparation of MgO–C refractory specimens

The raw materials used for preparing MgO–C specimens were fused magnesia (3–1 mm, 1–0.5 mm, 0.5–0 mm and < 45 μm, 98 wt% MgO, Dashiqiao, China), magnesia-rich spinel powder (~2 μm, 45 wt% MgO, 50 wt% Al_2O_3, Zhengzhou, China), silicon powder (< 45 μm, 98 wt% Si, Anyang, China), metallic aluminum (< 45 μm, 98 wt%, Xinxiang, China), flaky graphite (< 74 μm, 97.5 wt% fixed carbon, Qingdao, China) and as-prepared MgO–GONs composite powders. Thermosetting phenolic resins, one in liquid form (36 wt% of carbon yield, Zibo, China) and one in powder form (55 wt% carbon yield, Zibo, China) were used as binder. The batch containing 80 wt% fused magnesia, 6 wt% magnesia-rich spinel, 2 wt% Al powder, 1 wt% Si powder, 1 wt% flaky graphite and 10 wt% GON0 powders was used as a base composition for the MgO–C specimen designated as GN0. Different amounts of as-milled powders, namely, 10.2 wt% GON2, 10.5 wt% GON5, 10.8 wt% GON8 and 11 wt% GON10, respectively, were added into the base composition by replacing GON0 powders and the corresponding specimens were designated as GN2, GN5, GN8 and GN10, respectively. The amount of flaky graphite added in all the compositions was at such a level that the carbon content in the specimens was controlled at 1 wt%. Four weight percent liquid resin and 1 wt% resin powders were added into all the compositions. The preparation of MgO–C specimens was carried out by firstly mixing the raw materials for 30 min in a mixer with a rotating speed of 80–100 r/min. After kneading, bar shaped specimens (140 mm × 25 mm × 25 mm) were uniaxial pressed at 150 MPa and then cured at 200 °C for 24 h. Finally, the as-prepared specimens were fired at 1000 °C and 1400 °C in a sagger filled with coke grit. For all the specimens, the heating rate and holding time used were 5 °C/min and 3 h, respectively.

2.3. Tests and characterization methods

The bulk density (BD) and apparent porosity (AP) of the MgO–C refractory specimens obtained were measured according to Archimedes' Principle with kerosene as medium. Mechanical properties including cold modulus of rupture (CMOR) and flexural modulus (FM) were measured by the three-point bending test at ambient temperature with a span of 100 mm and a loading rate of 0.5 mm/min using an electronic digital control system (EDC 120, DOLI Company, Germany). The force–displacement curve of each refractory specimen was recorded simultaneously during the test. The phase composition and microstructures of the specimens were analyzed by means of X-ray diffraction (XRD, X'Pert Pro, Philips, Eindhoven, The Netherlands; using Ni filtered, Cu K_α radiation at a scanning speed of 2 °/min and a temperature of 289 K (16 °C)), field emission scanning electron microscopy (Nova 400 Nano FESEM, FEI Co., Philips, Eindhoven, The Netherlands) and energy dispersive X-ray spectroscopy (EDS, EDAX, Phoenix, Philips, Eindhoven, The Netherlands).

The thermal shock resistance of the specimens fired at 1400 °C was tested according to the following method. The specimens were heated in a coke bed up to 1100 °C with a heating rate of 5 °C/min, and soaked at this temperature for 30 min. Then, the specimens were taken out and quickly quenched into an oil bath; the purpose of using oil bath instead of water bath was to prevent oxidation and hydration of the specimens. This cycle was repeated 5 times. After 5 thermal shock cycles, the deterioration of the mechanical properties of the specimens was assessed by the three-point bending test. The residual strength ratio of

CMOR was calculated by the change in CMOR before and after the thermal shocks, i.e. the residual strength ratio of $CMOR = 100 \cdot CMOR_{TS}/CMOR$, where CMOR and $CMOR_{TS}$ were the CMOR before and after 5 thermal shock cycles, respectively.

In addition, the thermal expansion was measured via a thermal dilatometer (Unitherm™ model 1161 dilatometer system, Anter Corp., Pittsburgh, PA) from $\Phi 10\,mm \times 50$ mm column specimens cured at 200 °C; the measurement was made in an atmosphere of N_2 (99.9% N_2) to prevent oxidation of the specimens.

3. Results and discussion

3.1. SEM images of EG and MgO–GONs composite powders

Fig. 1 depicts the SEM micrographs of as-prepared EG. It can be seen that EG particles are worm-like and graphite layers have been opened mostly. Interestingly, the EG particle has a "bean pod" structure (Fig. 1a) with homogenous distances between balloons suggesting uniform expansion along the *c*-axis of graphite [22–24]. In addition, very thin GONs (in the range of 10–50 nm) were observed (Fig. 1b), indicating that the EG was an effective and reliable source for preparing the GONs.

The SEM images of MgO–GONs composite powders with different amounts of EG added are shown in Fig. 2. In general, the EGs with larger sizes were broken into pieces, which were distributed homogeneously in magnesia powders during ball milling. However, it was apparent that the GONs in the GON2 and GON5 specimens (Fig. 2a and b) were of much thinner thicknesses and smaller sizes (10–40 nm in thickness and 1–3 μm in size), while the GON8 and GON10 specimens (Fig. 2c and d) contained thicker and larger size of GONs (~100 nm in thickness and 3–8 μm in size) than in the GON2 and GON5 specimens, indicating that the EGs were more easily exfoliated when its content in the composite powders was lower.

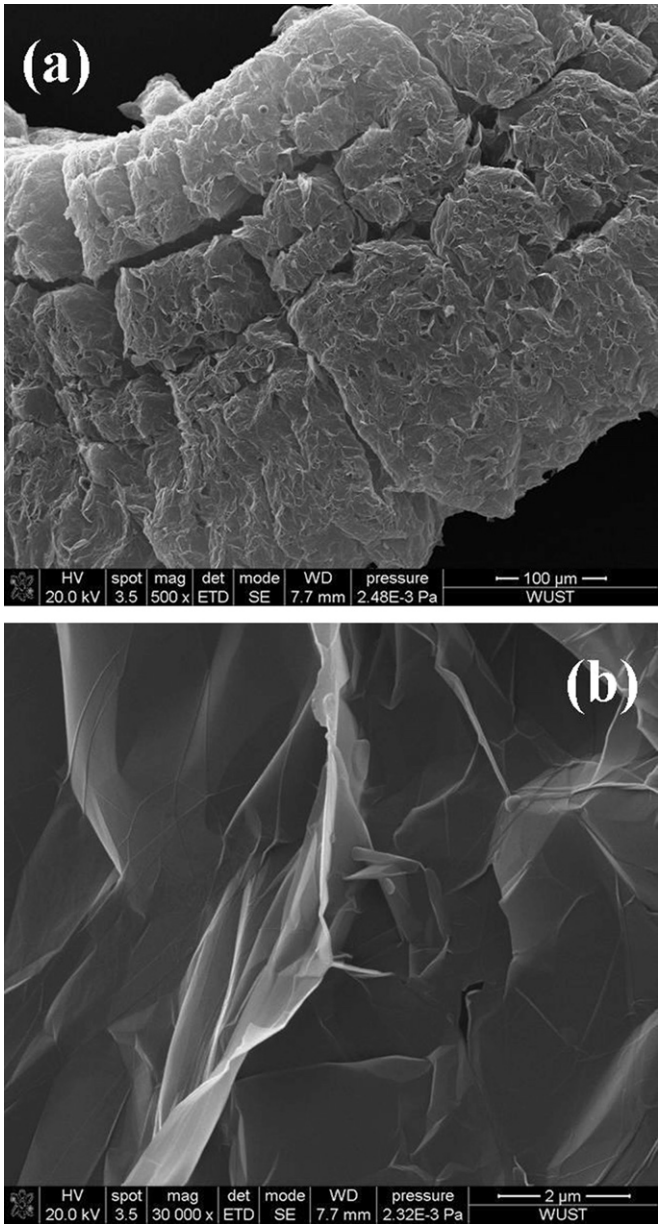

Fig. 1. SEM micrographs of EG: (a) magnification: 500× and (b) magnification: 30,000×.

3.2. The phase composition and microstructure of MgO–C refractory specimens

The XRD patterns were measured for all the coked specimens to examine the phase evolution in MgO–C refractory specimens during heating-up. It showed that no new phases were detected in the specimens coked at 1000 °C; the periclase, spinel, graphite and silicon phases detected were those present in the original raw materials (Fig. 3a). At 1400 °C, however, AlN and SiC phases formed while Si disappeared (Fig. 3b), but Al carbides such as Al_4C_3 and Al_2OC phases couldnot be detected in the MgO–C specimens owing to their less content [10]. In addition, it was noteworthy that the intensity of diffraction peak of graphite decreased gradually with the increasing of GONs addition, revealing that GONs had a lower degree of crystallinity than the flaky graphite [25,26]. It is also possible that some of the GONs added had taken part in the chemical reactions in MgO–C refractories, due to their higher activity than that of flaky graphite [27,28].

The microstructure of MgO–C refractories has been examined using a field emission scanning electron microscope (FESEM). In all the specimens coked at 1000 °C, a few of whiskers and octagonal shaped particles appeared in the matrix where aluminum powder particles were originally located. Moreover, these phases were much more easily found in the matrix of MgO–C refractories containing GONs. These whiskers and octagonal particles were identified as Al carbides and spinel by EDS analysis, respectively (Fig. 4). The results were in agreement with those reported by other investigators [1,10]. However, as

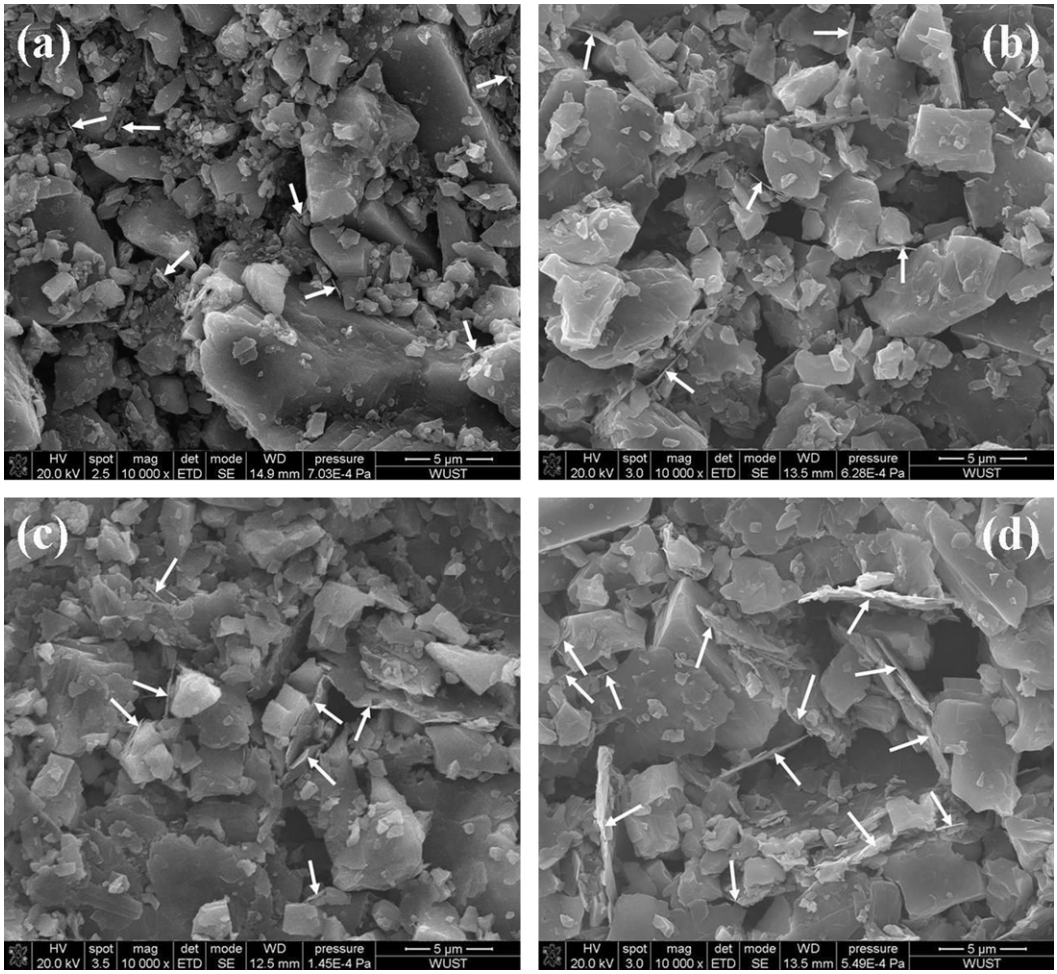

Fig. 2. SEM images of MgO–GONs composite powders: (a) GON2, (b) GON5, (c) GON8 and (d) GON10.

stated previously, these in-situ formed ceramic phases were not detected by XRD in the present study because the amount of the carbide phase formed was too low and the magnesium aluminate spinel was already present in the raw materials, whose diffraction peak overlapped with those of the in situ formed spinel phase.

With increase in temperature, large numbers of plate-like particles appeared in the matrix of MgO–C specimens coked at 1400 °C, which was in contrast to the whisker-like substances observed in the specimens coked at 1000 °C. With a combination of XRD and EDS analysis, these plate-like particles had been identified to be the AlN phase [29,30]. For the specimen GN0, the AlN phase interlocked with each other and was distributed only at the site where Al metal was originally present (Fig. 5a). However, for the specimens GN5 and GN10, in addition to the same microstructure features as those observed in the specimen GN0, some of AlN particles formed bonded to each other and were present in the pores and the matrix (Fig. 5c and e). Furthermore, thin GONs were observed in the specimen GN10 (Fig. 5e). Unfortunately, the SiC phase could not be easily differentiated from other in-situ formed ceramic phases in the specimens coked at this temperature, although it was detected by XRD.

Thermochemical calculations were also made using FactSage software to predict the phase evolution of MgO–C refractories during heating-up. The spinel powders added in the specimens were not considered in the calculations in order to clearly distinguish the evolution sequence of the reaction products of Al and Si in MgO–C specimens. The calculations were made for an atmosphere of 3.5×10^4 Pa CO and 6.5×10^4 Pa N_2 [1,31], and the parameter Alpha was set as the weight ratio of atmosphere gas to specimen. At 1000 °C (Fig. 6), both Al and Si are unstable phases. When Alpha is close to zero, the amounts of Al_4C_3 and SiC are high and $MgAl_2O_4$ and AlN contents close to zero. As Alpha increases, Al_4C_3 decreases whereas $MgAl_2O_4$ and AlN increase, and the amount of carbon (C) also increases slightly. The Al_4C_3 content abruptly drops to zero when Alpha increases to ~0.12. The amounts of $MgAl_2O_4$ and SiC decrease as Alpha increases, and then disappear at an Alpha value of ~0.15 and 0.215, respectively. Thereafter, with further increase in Alpha, Mg_2SiO_4 increases abruptly while Si_3N_4 increases firstly and then

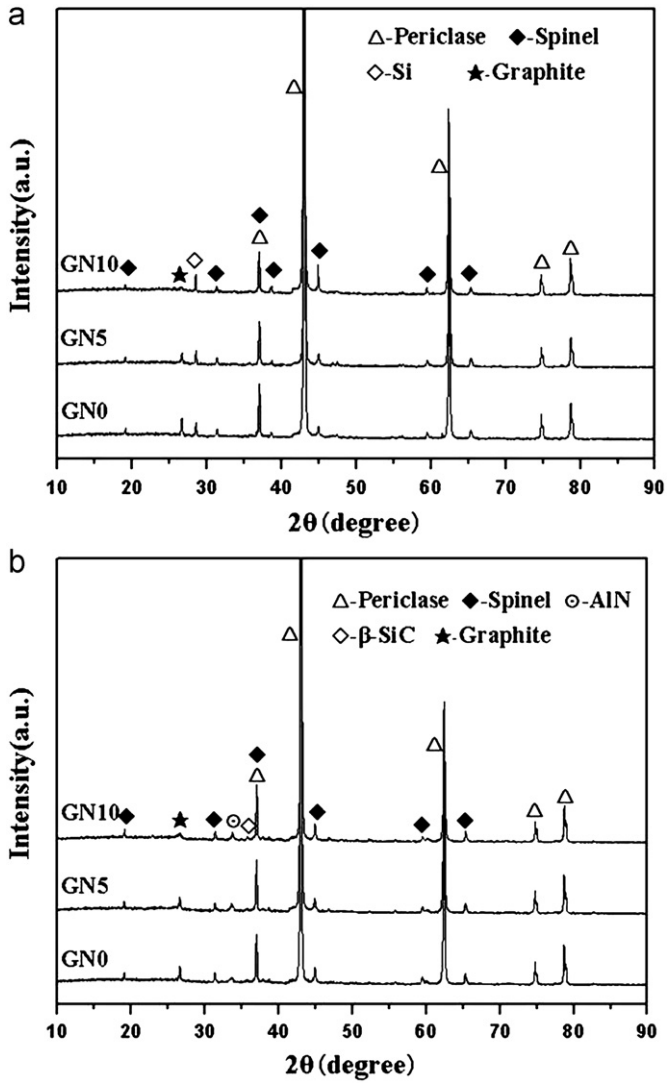

Fig. 3. XRD patterns of MgO–C refractory specimens fired at 1000 °C (a) and 1400 °C (b).

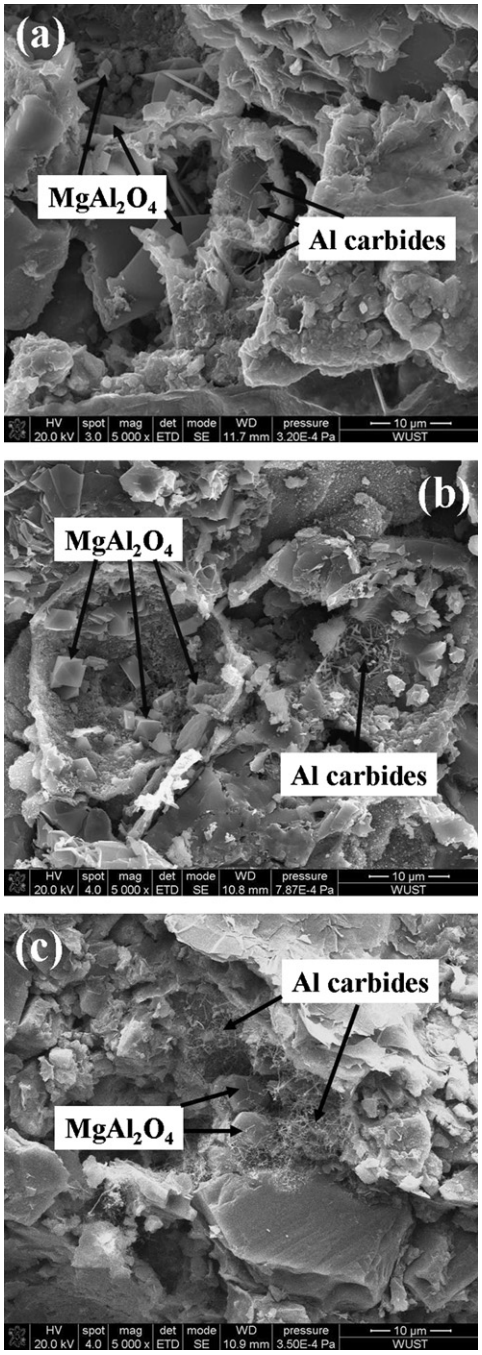

Fig. 4. SEM micrographs of MgO–C refractory specimens fired at 1000°C: (a) GN0, (b) GN5 and (c) GN10.

drops to zero when Alpha is at ~0.565. As increase in Alpha continues, Mg_2SiO_4 remains constant and $MgAl_2O_4$ increases continuously while AlN reduces. The partial pressures of N_2, CO and Mg (g) in the system, especially the partial pressure of Mg (g) are all at low values. Predicted phase changes at 1400 °C (Fig. 7) are similar to those at 1000 °C, except that the partial pressures of Mg (g) and CO are higher than at 1000 °C.

The predicted phases were consistent with the results of this study, although Si_3N_4 and Mg_2SiO_4 were not detected, which might be attributed either to the low amounts formed or to the restrictions of the kinetic factors [1,31]. In the meanwhile, it can be seen that the phase changes were related to the partial pressures of CO and N_2. For all the specimens fired at 1400 °C (Fig. 5), the AlN phase was observed in the microstructure, whereas the specimens containing the GONs showed more AlN phase distributed uniformly in the matrix. It was suggested that the GONs with higher activity might decrease the partial pressure of oxygen [27,28], leading to the increase in partial pressure of N_2 gas, which accelerated the diffusion of N_2 gas into the specimens and hence resulted in the formation of more AlN phase in the matrix.

3.3. The mechanical properties of MgO–C refractory specimens

Mechanical properties including CMOR and FM of MgO–C refractory specimens measured using the three-point

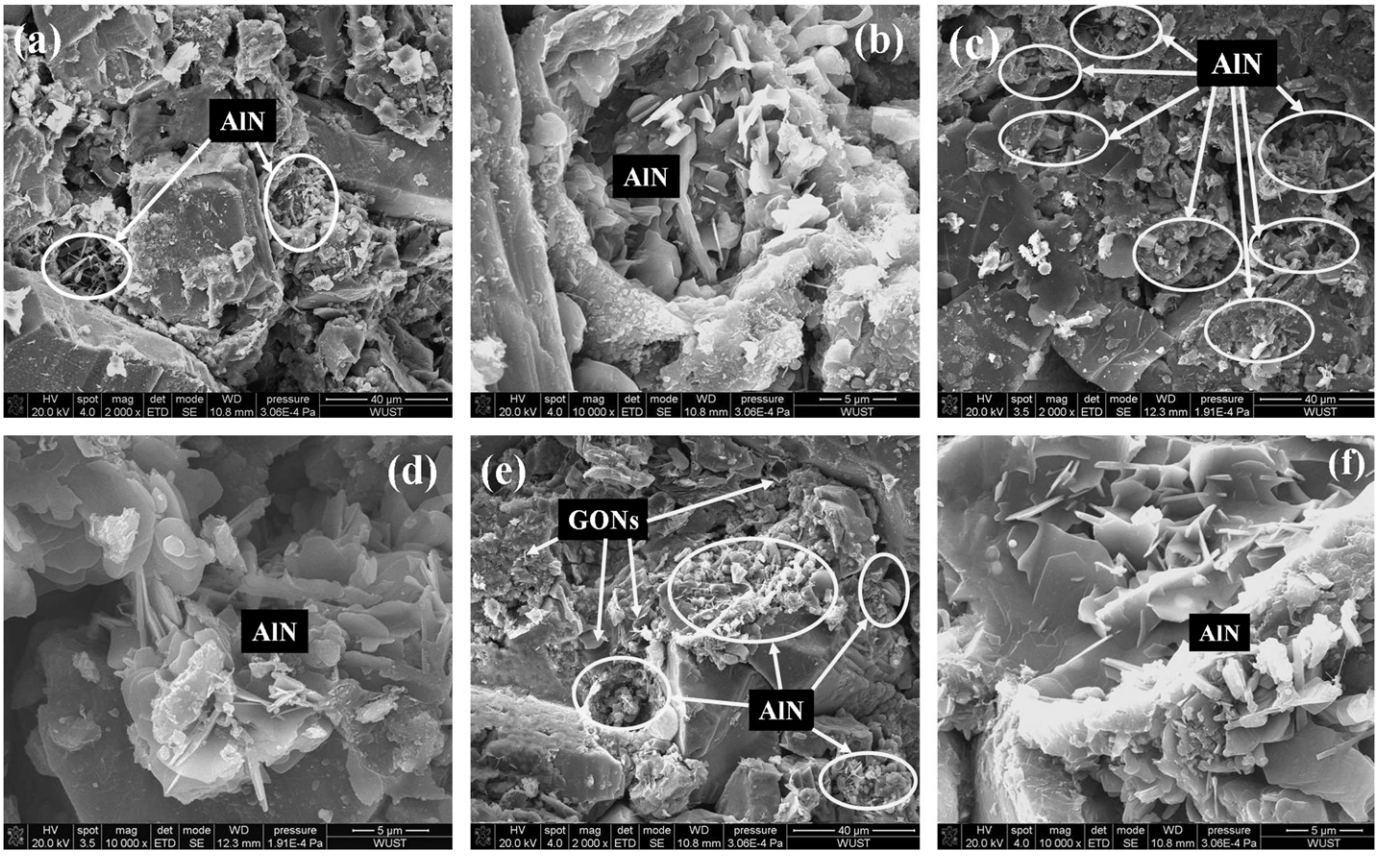

Fig. 5. SEM micrographs of MgO–C refractory specimens fired at 1400 °C: (a) and (b) GN0, (c) and (d) GN5, (e) and (f) GN10.

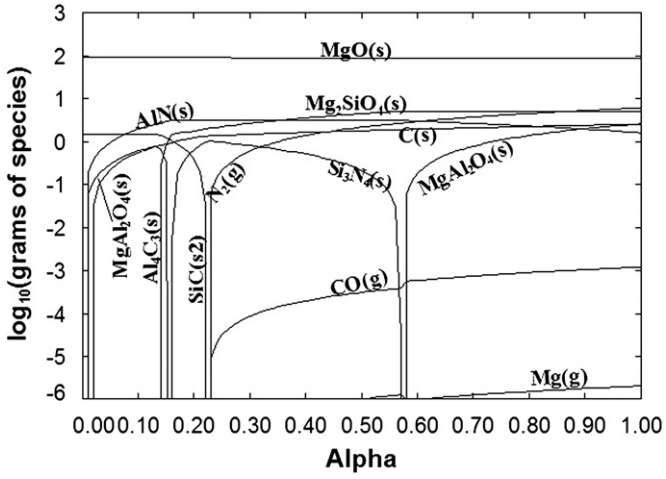

Fig. 6. Phase changes of MgO–C specimens fired at 1000 °C.

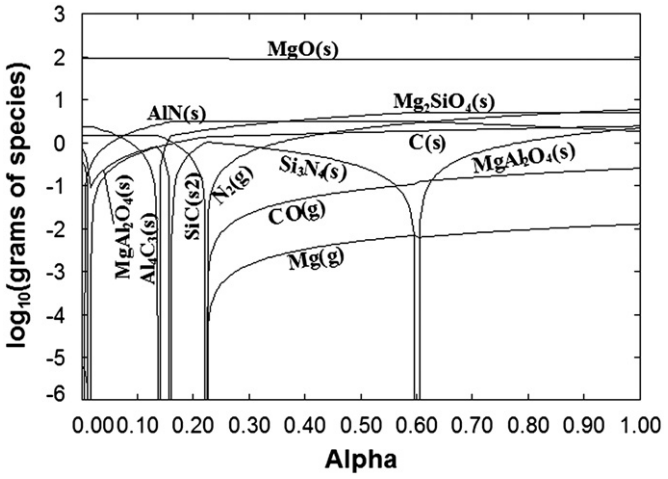

Fig. 7. Phase changes of MgO–C specimens fired at 1400 °C.

bending method are presented in Table 1. CMOR and FM of the specimens treated at 200 °C were the highest among the specimens treated at different temperatures, CMOR and FM of all the specimens containing GONs were lower than those for the specimen containing no GONs at this temperature, which was related to less compaction for specimens containing GONs (Table 2). However, CMOR and FM of all the specimens fired at 1000 °C decreased simultaneously because of the pyrolysis of the resins. As the coking temperature increased from 1000 °C to 1400 °C, CMOR of the specimens containing GONs increased and became higher than that of the specimen without GONs. Interestingly, the specimens GN2 and GN5 had higher CMOR and lower FM than the specimen GN0. For example, CMOR was 11.76 MPa for the specimen GN5 and 9.76 MPa for the specimen GN0 while FM was

Table 1
CMOR and FM of MgO–C refractory specimens treated at various temperatures.

Temperature	Index	GN0	GN2	GN5	GN8	GN10
200 °C	CMOR (MPa)	42.15	31.08	36.05	29.65	26.87
	FM (GPa)	7.27	6.60	7.03	6.33	5.75
1000 °C	CMOR (MPa)	10.69	9.69	10.60	8.57	7.75
	FM (GPa)	2.77	2.20	2.70	1.90	1.87
1400 °C	CMOR (MPa)	9.76	11.36	11.76	11.93	11.26
	FM (GPa)	2.72	2.70	2.64	2.82	2.81

Table 2
AP and BD of MgO–C refractory specimens treated at various temperatures.

Temperature	Index	GN0	GN2	GN5	GN8	GN10
200 °C	AP (%)	5.33	6.31	6.06	7.54	7.68
	BD (g cm^{-3})	3.04	3.03	3.03	3.01	3.01
1000 °C	AP (%)	11.63	11.97	12.99	13.13	12.81
	BD (g cm^{-3})	3.00	2.99	2.96	2.95	2.96
1400 °C	AP (%)	11.91	11.50	11.80	12.57	12.16
	BD (g cm^{-3})	2.99	3.00	3.00	2.97	2.97

2.64 GPa and 2.72 GPa for the specimens GN5 and GN0, respectively.

The force–displacement curves of MgO–C refractory specimens were influenced by heat-treated temperature and amounts of GONs added (Fig. 8). Among all the specimens, the specimens treated at 200 °C had the highest strength and displacement, which, however, decreased with the addition of GONs. With respect to the specimens coked at 1000 °C and 1400 °C, the specimens with 0.5 wt% GONs had the highest displacements and higher strengths. The improved mechanical properties may be attributed to the strengthening and toughening actions of the incorporated GONs on the one hand, the mechanisms of which included crack deflection, bridging, and pulling-out due to their homogeneous distribution in the material [19]. On the other hand, the ceramic phases such as AlN, Al_4C_3 and SiC, etc. interlocked with each other in the matrix, which provided much better mechanical properties for the specimens with the GONs added [1,10,32].

3.4. The thermal shock resistance of MgO–C refractory specimens

When the thermo-mechanical behavior of the coked specimens is concerned, which is normally characterized by the residual CMOR after 5 thermal shock cycles, all the compositions containing GONs exhibited higher residual strength compared to the composition without GONs (Fig. 9) although the thermal expansion of all the compositions was almost the same (Fig. 10). The specimen GN5 with 0.5 wt% GONs added had the highest residual strength ratio of 45.37%, but 37% for the specimen GN0, indicating that the addition of GONs was favorable to improve the thermal shock resistance of MgO–C refractories. It may be suggested that the homogeneous distribution of GONs and in-situ formation of much more ceramic phases in the matrix strengthened and toughened the MgO–C refractories. In fact, like EG, GONs have less oxidation resistance than that of natural flaky graphite due to their higher activity. So, the addition of GONs may have a negative influence on the oxidation resistance of MgO–C refractories depending on the amounts of GONs added, which will be considered in our later study.

4. Conclusions

MgO–GONs composite powders have been prepared and the microstructure and mechanical properties of MgO–C refractories made from the MgO–GONs composite powders have been investigated with following conclusions. Firstly, GONs of different sizes and thicknesses could be produced in magnesia powders by common wet-milling the EG and magnesia powder mixtures. Secondly, the addition of GONs had a positive influence on the mechanical properties of MgO–C refractories. Firing at 1400 °C resulted in much higher cold modulus of rupture and increased displacement for MgO–C specimens with GONs added in comparison with those that contained no GONs.

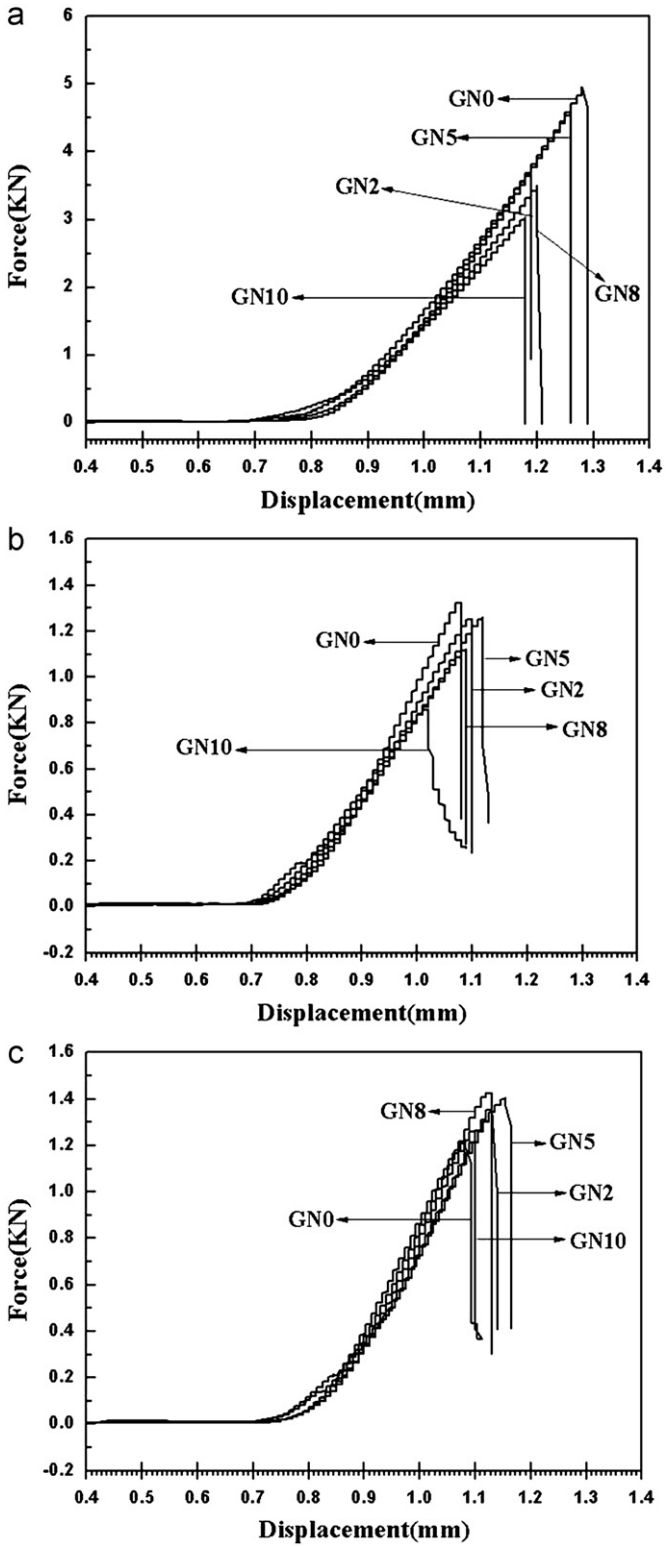

Fig. 8. Force–displacement curves of MgO–C refractory specimens treated at 200 °C (a), 1000 °C (b) and 1400 °C (c).

The thermal shock resistance of MgO–C refractories was improved with the addition of GONs, indicating that the GONs and in-situ formed ceramic phases in the matrix strengthened and toughened MgO–C refractories.

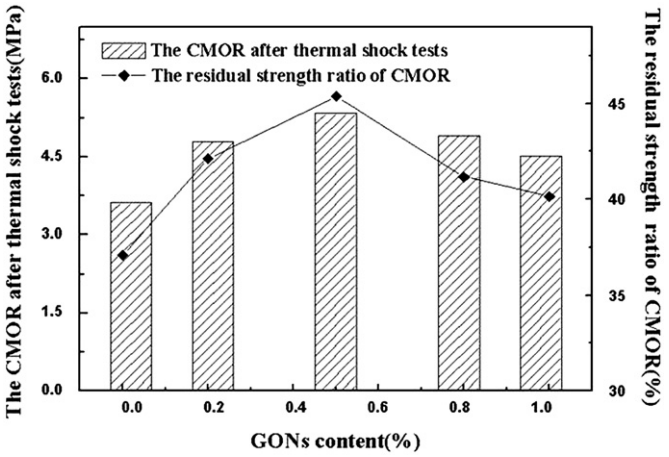

Fig. 9. Residual CMOR and the residual strength ratio of CMOR of the specimens after 5 thermal shocks.

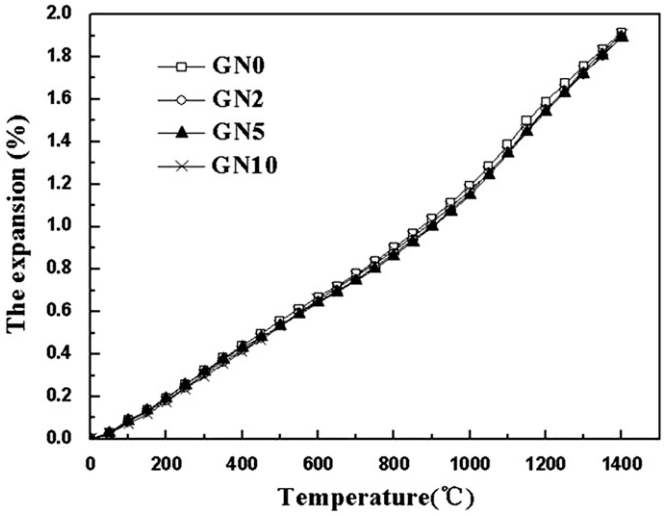

Fig. 10. Thermal expansion of the specimens cured at 200 °C.

Acknowledgments

The authors would like to thank the financial support from the National "973" Project of China (2012CB722702), the Natural Science Foundation of China (51002108), the Natural Science Foundation of Hubei Province (2009CDA050) and the programs of the New Century Excellent Talents in University (NCET-10–0137).

References

[1] S. Zhang, N.J. Marriott, W.E. Lee, Thermochemistry and microstructures of MgO–C refractories containing various antioxidants, Journal of the European Ceramic Society 21 (2001) 1037–1047.
[2] E. Mohamed, M. Ewais, Carbon based refractories, Journal of the Ceramic Society of Japan 112 (10) (2004) 517–532.
[3] I. Bae, M. Kim, D. Chung, M. Shin, Y. Seo, The improvement of MgO–C bricks toughness for RH snorkels, in: Proceedings of UNITECR'05 Congress, 8–11 November, Orlando, USA, 2005.

[4] S. Tamura, T. Ochiai, S. Takanaga, T. Kanai, H. Nakamura, Nano-tech. refractories-1: the development of the nano structural matrix, in: Proceedings of UNITECR'03 Congress, 19–22 October, Osaka, Japan, 2003, pp. 517–520.
[5] S. Takanaga, T. Ochiai, S. Tamura, T. Kanai, H. Nakamura, Nano-tech. refractories-2: the application of the nano structural matrix to MgO–C bricks, in: Proceedings of UNITECR'03 Congress, 19–22 October, Osaka, Japan, 2003, pp. 521–524.
[6] M. Hatta, S. Takanaga, O. Matsuura, T. Ochiai, S. Tamura, Nano-tech. refractories-5: the application of B_4C–C particles to MgO–C bricks, in: Proceedings of UNITECR'07 Congress, 18–21 September, Dresden, Germany, 2007, pp. 614.
[7] S. Takanaga, Y. Fujiwara, M. Hatta, T. Ochiai, S.Tamura, Nano-tech. refractories-3: development of "MgO-rimmed MgO–C brick", in: Proceedings of UNITECR'05 Congress, 8–11 November, Orlando, USA, 2005.
[8] H. Yasumitsu, M. Hirashima, O. Matsuura, S. Takanaga, T. Ochiai, S. Tamura, Nano-tech. refractories-9: the basic study on the formation of the nano structured matrix in MgO–C bricks, in: Proceedings of UNITECR'11 Congress, October 30–November 2, Kyoto, Japan, 2011.
[9] M. Bag, S. Adak, R. Sarkar, Study on low carbon containing MgO–C refractory: use of nano carbon, Ceramics International 38 (2012) 2339–2346.
[10] C.G. Aneziris, J. Hubalkova, R. Barabas, Microstructure evaluation of MgO–C refractories with TiO_2- and Al-additions, Journal of the European Ceramic Society 27 (2007) 73–78.
[11] M. Bavand-Vandchali, F. Golestani-Fard, H. Sarpoolaky, H.R. Rezaie, C.G. Aneziris, The influence of in situ spinel formation on microstructure and phase evolution of MgO–C refractories, Journal of the European Ceramic Society 28 (2008) 563–569.
[12] U. Klippel, C.G. Aneziris, Propects of ceramic nanoparticles as additives for carbon-boned MgO–C refractories, in: Proceedings of the 49th International Colloquium on Refractories, Aachen, Germany, 2006, pp. 6–9.
[13] S. Adak, A.S. Bal, A.K. Chattopadhyay, P.B. Panda, R.P. Rana, Effect of nano-titania addition of the properties of magnesia–carbon refractories, in: Proceedings of the 54th International Colloquium on Refractories, Aachen, Germany, 2011, pp. 180–183.
[14] B.Y. Ma, Q. Zhu, Y. Sun, J.K. Yu, Y. Li, Synthesis of Al_2O_3–SiC composite and its effect on the properties of low-carbon MgO–C refractories, Journal of Materials Science and Technology 8 (26) (2010) 715–720.
[15] Y. Matsuo, M. Tanaka, J. Yoshitomi, S. Yoon, J. Miyawaki, Effect of the carbon nanofiber addition on the mechanical properties of MgO–C brick, in: Proceedings of UNITECR'11 Congress, October 30–November 2, Kyoto, Japan, 2011.
[16] B.Z. Jang, A. Zhamu, Processing of nanographene platelets (NGPs) and NGP nanocomposites: a review, Journal of Materials Science 43 (2008) 5092–5101.
[17] J.R. Potts, D.R. Dreyer, C.W. Bielawski, R.S. Ruoff, Graphene-based polymer nanocomposites, Polymer 52 (2011) 5–25.
[18] R. Sengupta, M. Bhattacharya, S. Bandyopadhyay, A.K. Bhowmick, A review on the mechanical and electrical properties of graphite and modified graphite reinforced polymer composites, Progress in Polymer Science 36 (2011) 638–670.
[19] K. Wang, Y.F. Wang, Z.J. Fan, J. Yan, T. Wei, Preparation of graphene nanosheet/alumina composites by spark plasma sintering, Materials Research Bulletin 46 (2011) 315–318.
[20] Y. Fan, L.J. Wang, J.L. Li, S.K. Sun, F. Chen, L.D. Chen, W. Jiang, Preparation and electrical properties of graphene nanosheet/Al_2O_3 composites, Carbon 48 (2010) 1743–1749.
[21] P. Kun, O. Tapaszto, F. Weber, C. Balazsi, Determination of structural and mechanical properties of multilayer graphene added silicon nitride-based composites, Ceramics International 38 (2012) 211–216.
[22] J.H. Li, L.L. Feng, Z.X. Jia, Preparation of expanded graphite with 160 μm mesh of fine flake graphite, Materials Letters 60 (2006) 746–749.
[23] T. Wei, Z.J. Fan, G.L. Luo, C. Zheng, D.S. Xie., A rapid and efficient method to prepare exfoliated graphite by microwave irradiation, Carbon 47 (2008) 337–339.
[24] X.J. Yu, J. Wu, Q. Zhao, X.W. Cheng, Preparation and characterization of sulfur-free exfoliated graphite with large exfoliated volume, Materials Letters 73 (2012) 11–13.
[25] M.V. Antisari, A. Montone, N. Jovic, E. Piscopiello, C. Alvani, L. Pilloni, Low energy pure shear milling: a method for the preparation of graphite nano-sheets, Scripta Materialia 55 (2006) 1047–1050.
[26] Q.W. Tang, J.H. Wu, H. Sun, S.J. Fang, Crystallization degree change of expanded graphite by milling and annealing, Journal of Alloys and Compounds 475 (2009) 429–433.
[27] J.H. Han, K.W. Cho, K.H. Lee, H. Kim, Porous graphite matrix for chemical heat pumps, Carbon 36 (12) (1998) 1801–1810.
[28] J.G. Zhao, Q.G. Guo, J.L. Shi, L. Liu, J.S. Jia, Y.C. Liu, H.Q. Wang, Carbon nanotube growth in the pores of expanded graphite,by chemical vapor deposition, Carbon 47 (2009) 1747–1751.
[29] Y.W. Li, S.L. Jin, G.T. Liu, W.H. Zhang, J.Q. Ao, Z.Y. Li, Behavior of magnesium and silicon in the formation of MgO/AlN composite, Journal of Materials Science 44 (2009) 4155–4161.
[30] S.S.S. Kumari, U.T.S. Pillai, B.C. Pai, Synthesis and characterization of in situ Al–AlN composite by nitrogen gas bubbling method, Journal of Alloys and Compounds 509 (2011) 2503–2509.
[31] Xilai Chen, Yawei Li, Yuanbing Li, Shengli Jin, Lei Zhao, Gee Shan, Effect of temperature on the properties and microstructures of carbon refractories for blast furnace, Metallurgical and Materials Transactions A—Physical Metallurgy and Materials Science 40A (2009) 1675–1683.
[32] H.B. Fan, Y.W. Li, S.B. Sang, Microstructures and mechanical properties of Al_2O_3–C refractories with silicon additive using different carbon sources, Materials Science and Engineering A 528 (2011) 3177–3185.